Transmission and reflection mode macroscopic x-ray powder diffraction imaging for the noninvasive visualization of paint degradation in still life paintings by Jan Davidsz. de Heem

Article

Transmission and reflection mode macroscopic X ray powder diffraction (MA XRPD) imaging for the noninvasive visualization of paint degradation in still life paintings by Jan Davidsz. de Heem

Frederik Vanmeert, Nouchka De Keyser, Annelies van Loon, Lizet Klaassen, Petria Noble, and Koen Janssens

Anal. Chem., **Just Accepted Manuscript** • DOI: 10.1021/acs.analchem.9b00328 • Publication Date (Web): 10 May 2019

Transmission and reflection mode macroscopic X-ray powder diffraction (MA-XRPD) imaging for the noninvasive visualization of paint degradation in still life paintings by Jan Davidsz. de Heem

Frederik Vanmeert,[‡*] Nouchka de Keyser,[‡†§] Annelies van Loon,[†] Lizet Klaassen,[§] Petria Noble,[†] and Koen Janssens[‡]

[‡] AXES Research Group, Department of Chemistry, University of Antwerp, Groenenborgerlaan 171, B-2020 Antwerp, Belgium

[†] Paintings Conservation, Rijksmuseum, Museumstraat 1, 1071 XX Amsterdam, the Netherlands

[§] Paintings Conservation, Royal Museum of Fine Arts Antwerp, Lange Kievitstraat 111-113 bus 100, 2018 Antwerp, Belgium

ABSTRACT: The use of noninvasive chemical imaging techniques is becoming more widespread for the study of cultural heritage artefacts. Recently a mobile instrument for macroscopic X-ray powder diffraction (MA-XRPD) scanning was developed, which is capable of visualizing the distribution of crystalline (pigment) phases in quasi-flat painted artefacts. In this study, MA-XRPD is used in both transmission and reflection mode for the analysis of three 17th century still life paintings: two paintings by Jan Davidsz. de Heem (1606-1684) and one copy painting after De Heem by an unknown artist. MA-XRPD allowed to reveal and map the presence of *in situ* formed alteration products. In the works examined, two rare lead arsenate minerals, schultenite ($PbHAsO_4$) and mimetite ($Pb_5(AsO_4)_3Cl$) were encountered, both at and below the paint surface; they are considered to be degradation products of the pigments realgar (α-As_4S_4) and orpiment (As_2S_3). In transmission mode, the depletion of lead white, present in the (second) ground layer, could be seen, illustrating the intrusive nature of this degradation process. In reflection mode, several sulfate salts, palmierite ($K_2Pb(SO_4)_2$), syngenite ($K_2Ca(SO_4)_2.H_2O$) and gypsum ($CaSO_4.2H_2O$), could be detected, in particular at the (top) surface of the copy painting. Estimates for the information depth and sensitivity of both transmission and reflection mode MA-XRPD for various pigments have been made. The possibility of MA-XRPD to allow for noninvasive identification and visualization of alteration products is considered a significant advantage and unique feature of this method. MA-XRPD can thus provide highly relevant information for assessing the conservation state of artworks and could guide possible future restoration treatments.

In the field of cultural heritage, the identification of paint materials (e.g., organic dyes, inorganic pigments and binding media) plays a vital role in solving questions regarding restoration, conservation, dating, and authentication of works of art and understanding an artist's *modus operandi*. Furthermore, to evaluate an object's conservation state additional information regarding the *in situ* formation of secondary products is required. Degradation phenomena, and the subsequent discoloration or loss of structural integrity of paint layers that they entail, are often the result of intricate physicochemical processes that are taking place within or at the surface of paint layers. They are triggered by either internal factors, such as the co-presence of mutually incompatible pigment or pigment/binder mixtures, or external factors, such as environmental conditions (relative humidity, light, and temperature), biological activity, volatile organic compounds, pollution or human interventions, or both.[1]

In order to gain more profound insights into the nature and relative importance of these phenomena as well as characterize the layer build-up of painted works of art, typically (a small number of) minute paint samples are collected from an artwork. After preparation as cross-sections, these can then be investigated with multiple nondestructive analytical (point-based and microimaging) techniques, such as scanning electron microscopy coupled to energy dispersive X-ray spectroscopy (SEM-EDX),[2] micro Raman[3] and micro Fourier transform infrared (μ-FTIR) spectroscopy[4]. In recent years, also various forms of synchrotron radiation based X-ray techniques have been employed for this purpose.[5,6] Although these samples can be a source of highly detailed stratigraphic information, they originate from only a limited number of (possibly unrepresentative) locations on the artwork.

In recent years, both elemental and chemical imaging techniques, capable of visualizing the (often) heterogeneous composition of painted objects on a macroscopic scale, have been developed in order to expand these detailed analyses to entire objects and to include artworks that might be prohibited from sampling.[7] In this respect, macroscopic (MA-)XRF and visible/near infrared (VNIR) reflectance imaging have so far been the most used spectroscopic imaging techniques, respectively delivering distribution images based on elemental or molecular features.[8,9] Their significance to the cultural heritage field is evidenced by their numerous applications: improved visualization of underdrawings and compositional paint changes as well as identification and mapping of artists' materials (e.g., pigments and binding medium).[10-12] To a lesser extent, also macroscopic FTIR scanning in reflection mode (MA-rFTIR), has recently been described.[13] While frequently

employed for imaging of microscopic cross-sections, *in situ* Raman imaging on the macro scale remains quite rare.[14,15] However, obtaining information about *in situ* formed alteration products using these noninvasive imaging techniques remains elusive.

Although originally developed at synchrotron radiation facilities, macroscopic X-ray powder diffraction scanning (MA-XRPD) has been successfully converted to a laboratory technique using conventional X-ray sources in transmission mode (i.e. X-ray source and detector are on opposite sides of the painting).[16-18] MA-XRPD allows for the direct identification and visualization of complex mixtures of crystalline compounds on painted works of art. On *Sunflowers,* the iconic painting by Van Gogh (Van Gogh Museum, Amsterdam, NL), the technique was able to visualize different chrome yellows subtypes favored by Van Gogh, $PbCrO_4$ and $PbCr_{1-x}S_xO_4$ which exhibit a strongly different sensitivity to light; also information on the orientation of the pigment crystals within individual brush strokes could be obtained.[19] Furthermore, MA-XRPD allowed to distinguish between superimposed pigments applied on the *recto* or *verso* side of an illuminated manuscript by exploiting the (minute) shift in diffraction signals.[20]

Recently a small mock-up painting has been imaged in reflection mode (i.e. X-ray source and detector are located on the same side of the painting) illustrating that in reflection mode, MA-XRPD is mostly sensitive to superficial information (e.g., thin paint layers at the top surface), while transmission mode yields information that is averaged along the entire painting structure.[21] This makes reflection mode MA-XRPD and interesting candidate for the direct noninvasive study of alteration products as they are frequently formed as thin superficial layers on the artwork. However, in reflection mode the X-ray source impinges the painting under a small angle (around 10°) causing the beam footprint to be spread out over a larger area and therefore reducing the spatial resolution.

In the present paper, we employed MA-XRPD in both transmission and reflection mode to visualize degradation products that formed *in situ* inside the paint layer structure or on the surface of three 17th century oil on canvas paintings: *Flowers and Insects* (1660-1670), Royal Museum of Fine Arts Antwerp, and *Festoon of Fruit and Flowers* (1660-1670), Rijksmuseum Amsterdam, by Jan Davidsz. de Heem (1606-1684), and a copy painting after De Heem, *Still Life with Fruit and a Lobster* (1665-1700), Rijksmuseum Amsterdam, by an unknown artist, see Figure 1. These works were part of a study into the painting techniques of still life paintings by De Heem.[22] Therefore, complementary information was available to correlate with the data obtained with MA-XRPD. To strengthen the interpretation of the obtained compound-specific distribution images, it is relevant to briefly consider the sensitivity and information depth of MA-XRPD for various inorganic pigments in both experimental modes.

MATERIAL AND METHODS

MA-XRF/XRPD

The imaging experiments were carried out using a mobile MA-XRF/XRPD scanning instrument operating in transmission and reflection mode, see Figure S-1.

In transmission mode, a low power X-ray micro source (44 W, IμS-Ag^{HB}, Incoatec GmbH, DE) was employed, delivering a monochromatic (Ag-K_α; 22.16 keV) and focused X-ray beam with a photon flux of 1.1 10^7 photon s^{-1} (focal spot diameter: 112 (3) μm; output focal distance: 21.6 (1) cm; divergence: 3.8 (3) mrad). Diffraction patterns were recorded with a PILATUS 200K area detector (Dectris Ltd., CH) placed perpendicular to the source at the backside of the painting. The distance between the painting and the area detector was around 11.5 cm, while the distance between the X-ray source collimator and the painting was around 2.5 cm. The area detector is placed at the output focal distance, so that the diameter of the resulting beam footprint on the painting is around 0.4 mm.

In reflection mode, it becomes difficult to detect diffraction signals at small 2θ angles because of geometrical constraints. For this reason a similar X-ray micro source (30 W, IμS-Cu, Incoatec GmbH, DE), but with a lower primary excitation energy (Cu-K_α; 8.04 keV) was used as this results in larger scattering angles for the same crystalline material. The source specifications in reflection mode are the following: focal spot diameter of 313 (5) μm, output focal distance of 39.8 (1) cm, divergence of 2.6 (4) mrad and flux of 7.0 10^8 photons s^{-1}. An incident angle of 8° was chosen between the primary X-ray beam and the painting's surface, resulting in an enlarged beam footprint of around 2 mm in the horizontal direction; in the vertical direction the beam dimension is around 0.3 mm. The PILATUS detector was positioned on the front side of the artwork with an angle below 30° between the area detector and the painting at a distance of around 0.5 cm from the painted surface. To reduce the effects of local topography and curvature of the painting's surface on the collected diffraction data, the distance between the artwork and the instrument was automatically adjusted with a laser distance sensor (Baumer GmbH, DE) at each measurement point in the scanning process.

In both modes the instrument was equipped with a Vortex-Ex SDD detector (SII, US), collecting X-ray fluorescence radiation from the front side of the painting. The artworks were placed on an easel and mounted on top of three motorized stages to allow for the scanning movement (max. range: 10 cm x 25 cm x 10 cm, Newport Corporation, US). Calibration of several instrumental parameters was performed with a LaB_6 standard for powder diffraction (SRM 660, NIST) or with a calcite paint layer for respectively the transmission and reflection mode.

Processing of the diffraction data and visualization of the crystalline phase distributions was performed using the XRDUA software following a procedure that has been described elsewhere.[20,23] The diffraction data collected in transmission mode on *Flowers and Insects* and *Still Life with Fruit and a Lobster* has been corrected for minor misalignment of the painting which improves the quality of the distribution images. For this purpose, the apparent shifts in the 2θ pattern of respectively hydrocerussite and cerussite were used as internal markers to track and correct for the small displacements of the painting relative to the XRD detector.[20] The PyMca software package was used for processing of the X-ray fluorescence spectral data.[24] To improve the readability of the final MA-XRF and MA-XRPD distribution images, pixels at the outer edges of the gray scale histograms were avoided by stretching the linear distribution of the white levels using GIMP 2.

Information depth and sensitivity

Depending on the geometry of the MA-XRF/XRPD instrument, information from different depths below the paint surface is obtained. For this reason the information depth of MA-XRPD in reflection mode has been estimated for various pigments. Additionally, the relative diffracted intensity has been estimated to obtain an indication of the relative sensitivity

of the MA-XRF/XRPD instrument for various painters' materials. A detailed description of these estimations and their results are given in the supporting information.

In transmission mode, the entire painting structure, from the varnish down to the individual paint layers, ground and canvas, is probed by the X-ray beam. In this way, only crystalline material that is either abundantly present throughout the layer structure (e.g., the main component of a thick ground), or that exhibits a high scattering power (e.g., pigments that contain heavy elements, such as Pb and Hg, see Table S-2) will dominate the diffraction results. On the other hand, reflection mode MA-XRPD is more suited for gathering information on (thin) surface layers. In this mode, the X-ray beam impinges upon the painting under a small angle with the surface, resulting in a shallow probing depth: typically < 10 µm and < 50 µm for pigments containing respectively 'heavy' (e.g., Pb, Hg) and 'light' (e.g., Ca, Cu, Zn) elements, see Table S-3. In this manner, the relative sensitivity for materials located at the top surface benefits greatly since the (often thick) ground layer is prevented from dominating the diffraction data.

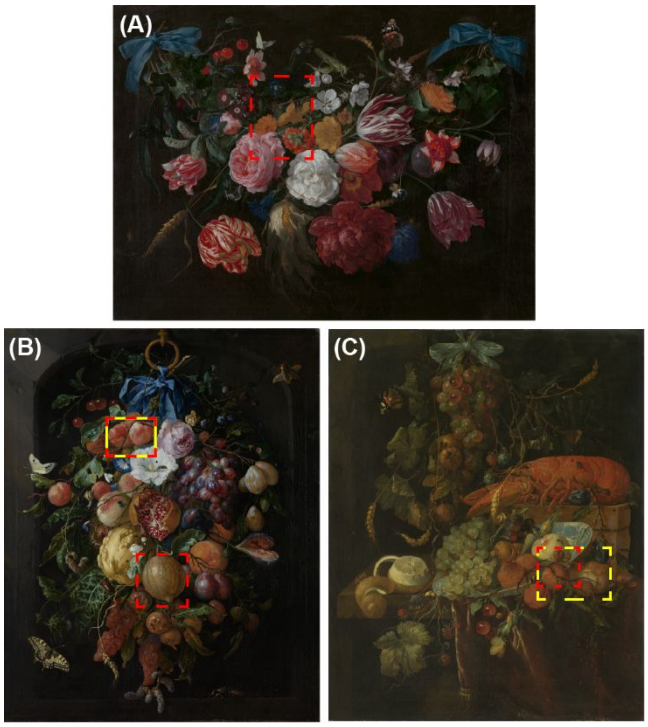

Figure 1. (A) Jan Davidsz. de Heem, *Flowers and Insects*, 49 x 67 cm, oil on canvas, 1660-1670, Royral Museum of Fine Arts Antwerp (inv. no. 54), BE, © KMSKA, Lukas - Art in Flanders VZW, Photo: Dominique Provost, (B) Jan Davidsz. de Heem, *Festoon of Fruit and Flowers*, 73.4 x 59.6 cm, oil on canvas, 1660-1670, Rijksmuseum (inv. no. SK-A-138), NL, © Rijksmuseum, and (C) unknown artist, copy after Jan Davidsz. de Heem, *Still Life with Fruit and a Lobster*, 70 x 59 cm, oil on canvas, 1665–1700, Rijksmuseum (inv. no. SK-A-139), NL, © Rijksmuseum. Dashed boxes mark the areas imaged with MA-XRF/XRPD in transmission (red) and reflection mode (yellow).

Still Life paintings

Flowers and Insects is a well-preserved oil painting on canvas by the 17th century Dutch painter Jan Davidsz. de Heem dated between 1660-1670 (Royral Museum of Fine Arts in Antwerp). It depicts a garland fastened with two blue ribbons displaying various types of flowers, such as tulips, Persian roses, orange marigolds and morning glories, cherries and insects. *Festoon of Fruit and Flowers* by Jan Davidsz. de Heem (Rijksmuseum), executed on a plain weave canvas, has been wax resin lined. This festoon, held together by a blue ribbon, comprises a multitude of fruits, flowers and insects. Below the central pomegranate, a large lemon with greyish-yellow skin is visible. Above the pomegranate, several apricots are part of the composition. The painting *Still life with Fruit and a Lobster* (Rijksmuseum) is part of a series of copies after the signed original in the Gemäldegalerie Alte Meister in Dresden, dated around 1669. Formerly, it was considered an autograph old copy of the master, however there were some substantial differences noted between the painting technique of this painting and Jan Davidsz. de Heem.[25] The still life displays a red lobster meticulously surrounded by a festoon and a wan-li dish filled with fruits on a purplish velvet tablecloth. The yellowish appearance of this painting is the result of a discolored coat of varnish.

Because of the inherent low sensitivity of XRPD, when compared to XRF, relatively long dwell times (typically 10 s point^{-1}) are required. This limits the size of the areas that can be imaged within a reasonable timeframe. Therefore, a selection of areas showing signs of discoloration was made based on previous examinations. In total, four different areas were analyzed with MA-XRF/XRPD in transmission and/or reflection mode as shown in Figure 1. Step sizes between 1 and 2 mm in both horizontal and vertical directions were employed (see Table S-1 for details on all area scans).

RESULTS AND DISCUSSION

Ground and pigment usage

Previous cross-section examination showed the presence of a double ground for the three paintings.[22] The bottom layer for *Flowers and Insects* and *Festoon of Fruit and Flowers* has a reddish-brown color and is mainly composed of fine grained red earth pigments and chalk, while the thicker upper ground, with a warm greyish-brown color, contains a mixture of lead white, earth pigments and chalk. A different composition for the ground layers was found for *Still Life with Fruit and a Lobster*. Here, a coarsely grained first layer composed of chalk, red earth pigments and large lead white particles, is followed by a thinner grey layer with lead white and bone black particles.

The effect of the double ground layer on the transmission mode MA-XRPD results for *Festoon of Fruit and Flowers* is visible in Figure 2. It can be seen that the distributions of lead white (mostly hydrocerussite, $2PbCO_3.Pb(OH)_2$) and chalk (calcite, $CaCO_3$) are dominated by their presence in the double ground as only the white flower in the bottom right corner links the hydrocerussite distribution to the optical photograph. The bottom ground layer, rich in calcite, clearly shows the weave structure of the canvas, which is less pronounced in the hydrocerussite distribution present in the upper ground layer (calcite and hydrocerussite MA-XRPD maps). In reflection mode, the calcite distribution highlights the green foliage, the acorns and paler areas of the apricots, where chalk has likely been used as a substrate for a yellow lake. In *Still Life with Fruit and a Lobster*, calcite is found throughout the orange-brown shadow of the wooden box supporting the lobster and in the yellow of the peach, strongly contrasting its near absence in transmission mode (calcite MA-XRPD maps in Figure S-4).

This indicates that while calcite is not or only sparingly used in the ground of the copy painting, it is a prominent constituent of (some of) the (upper) paint layers. A similar finding can be seen for cerussite ($PbCO_3$), which was only poorly present in the transmission measurements of *Festoon of Fruit and Flowers*, but shows a clear presence in the reflection measurements (cerussite MA-XRPD maps Figure 2). In the copy painting both cerussite and hydrocerussite are found to dominate the diffraction data in transmission mode, showing the different composition of the lead white used for the grounds of *Still Life with Fruit and a Lobster*.

To achieve the lifelike rendering of the different textures of the fruits and flowers, De Heem and his contemporaries disposed of a large set of painter's materials and artistic techniques. Table 1 provides a summary relating color, pictorial elements and main pigments employed in the paintings under investigation. Most of these data were previously obtained by means of MA-XRF in combination with microscopic observation and microanalysis of paint samples.[22]

With MA-XRPD it can be seen that the red vermilion (cinnabar, HgS) has been used in the pictorial layers of the apricots and is visible in both transmission and reflection mode (cinnabar MA-XRPD maps in Figure 2 and Figure S-4). Because of its high scattering power this pigment is still clearly visible in transmission mode (see Table S-2). On the other hand, the blue color used in the three paintings for the blue ribbon and the morning glories or for the blue plums and the wan-li dish contains ultramarine, see lazurite MA-XRPD maps in Figure 2 and Figure S-4, which, owing to its very low scattering power, is not visible in transmission mode.

Table 1. Overview of pigments used in the three still life paintings based on previous investigations [22]

Color	Pictorial elements	Main inorganic pigment	Additional pigments/dyes
White	Roses, Irises, Lilies	Lead white $2PbCO_3.Pb(OH)_2$ $PbCO_3$	Chalk
Red	Tulips, Carnations, Roses	Vermilion HgS	Red lakes, Lead white
Yellow	Lemons, Roses	Orpiment As_2S_3	Lead tin yellow, Yellow lakes, Earth pigments
	Corn ear, Acorns	Yellow ochre FeO(OH)	Yellow lakes
Orange	Peaches, Apricots, Marigolds	Realgar As_4S_4	Earth pigments, Orpiment, Vermilion
Blue	Ribbons, Cornflowers, Plums	Ultramarine $Na_4Ca_4Al_6Si_6O_{24}S_2$	
Green	Foliage	Blue verditer $2CuCO_3.Cu(OH)_2$	Yellow lakes, Lead tin yellow
Black	Background	Carbon black C	Bone black

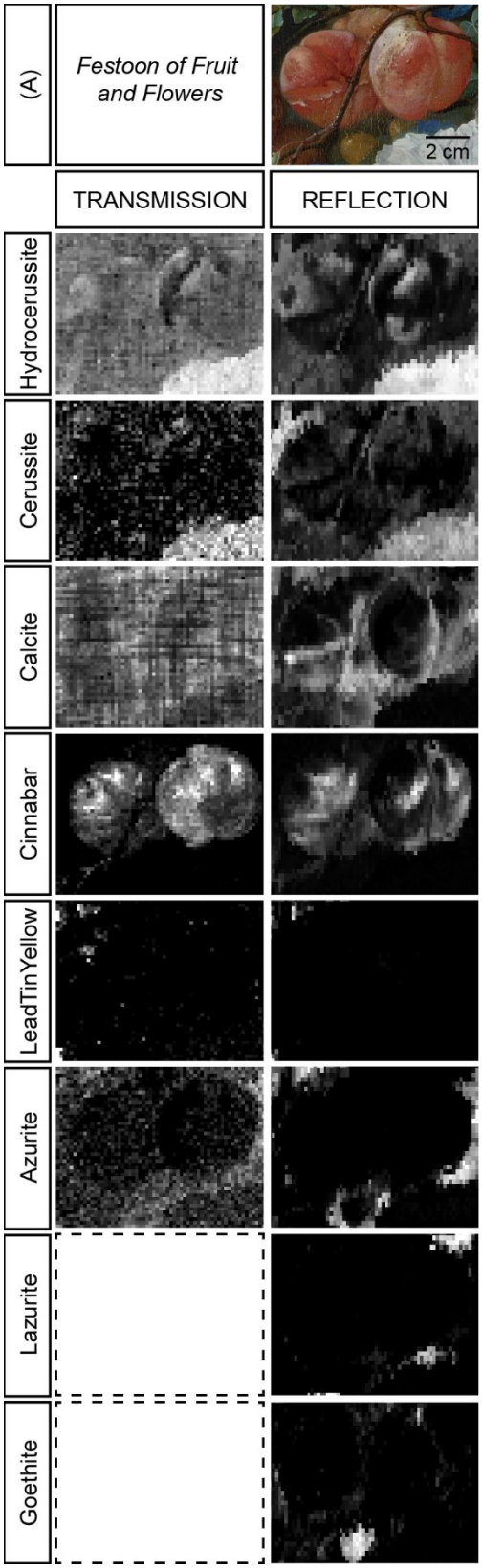

Figure 2. Compound-specific distribution images obtained with MA-XRPD from a detail of the apricots in *Festoon of Fruit and Flowers* in both (left) transmission and (right) reflection mode. Brighter colors indicate a higher scaling parameter. Empty dashed boxes indicate compounds that were not detected. Experimental parameters are given in Table S-1. (A) Optical photograph of the analyzed area.

For the white flowers and highlights, the lead white pigment with various compositions of hydrocerussite and cerussite has been used. This is apparent in the distributions obtained in reflection mode as the strong contribution of lead white present in the ground layers is avoided.

Blue verditer, a synthetic copper carbonate ($2CuCO_3.Cu(OH)_2$), is present in the green foliage together with lead-tin yellow (type I, Pb_2SnO_4) for the brighter greens (azurite and lead tin yellow MA-XRPD maps in Figure 2) and is also more clearly visible in reflection mode. While synthetic blue verditer is crystallographically indistinguishable from azurite, light microscopy and SEM analysis revealed a distinct spherical particle shape that is different from the crushed crystal shards expected for the natural azurite pigment.[22] For this painting, the final green color was obtained by mixing the blue verditer with smalt (Co MA-XRF map, not shown), and a yellow lake.[22]

Additionally also earth pigments, such as yellow and red ochre (respectively goethite and hematite), were found in reflection mode, (goethite and hematite MA-XRPD maps in Figure 2 and Figure S-4), which cannot be discriminated using only MA-XRF. While cross-sectional analyses have shown the presence of these iron-based pigments in the ground layers, they were not detected with MA-XRPD in transmission mode. This is the result of a low amount of crystalline material combined with the relatively low sensitivity of MA-XRPD for these iron-based pigments (see Table S-2).

Interestingly, the transmission results show Naples yellow to be present in the peach of *Still Life with Fruit and a Lobster* (bindheimite MA-XRPD map in Figure S-4), however this is not detected in the reflection measurements; in its turn, lead-tin yellow is now clearly present (lead tin yellow MA-XRPD map in Figure S-4). Indeed, two different yellow layers were used to create the yellow color of the peach: a top layer (around 10 μm) containing lead-tin yellow, and an underlying thicker layer containing Naples yellow (see Figure S-5).[26] The difference in the results between the two geometries relates to the different information depth that is probed: the thickness of the upper paint layer, containing lead-tin yellow, is of the same thickness as the information depth for this pigment in reflection mode (< 10 μm, see Table S-3), so that Naples yellow from the underlying layer can no longer be detected. Care should thus be taken when interpreting results obtained in reflection mode, since overlying layers can easily block other pictorial or preparatory layers that lie underneath.

Although the differences found between the two original De Heem paintings and the copy painting in terms of pigment usage remains limited, both below and on top of the pictorial paint layers various different alteration products could be revealed by means of MA-XRPD.

Degradation phenomena

Lead arsenates

Arsenic is found in various fruits and flowers depicted throughout the different still life paintings (e.g., in the apricots, the marigold flower, the yellow Persian rose and the lemon) as shown by the As-K MA-XRF maps in Figure 3 and Figure S-6. The presence of arsenic suggests that the artists made use of either the yellow orpiment (As_2S_3) or the orange-red realgar (α-As_4S_4). However, these arsenic sulfide pigments were not detected with MA-XRPD. Instead two rare lead arsenate minerals are encountered: schultenite ($PbHAsO_4$) and mimetite ($Pb_5(AsO_4)_3Cl$) as shown in the schultenite and mimetite MA-XRPD maps of Figure 3 and Figure S-6 (see also Figure S-7). The presence of these unusual lead arsenates on the surface of these oil paintings is intriguing, as only a handful reports mention these compounds in works of art, and none concern oil paintings.

Reports on the occurrence of the yellow mineral mimetite as a paint material are limited to three Hellenistic steles from Alexandria[27,28] and several murals.[29-31] In the heavily degraded murals of the church of St. Gallus in Northern Bohemia (13th century) mimetite is thought to be a degradation product formed from the interaction between orpiment and red lead (Pb_3O_4).[32] The occurrence of schultenite seems even more unique, but has recently been reported as a degradation product of orpiment, together with arsenolite (As_2O_3), on a colonial American polychromed chest on stand.[33]

Both orpiment and realgar are known to be sensitive to light, causing a fading of their color.[34] This is the result of the photo-oxidation to arsenolite, either directly as is the case for orpiment, or through an intermediate, pararealgar (As_4S_4), for realgar.[34,35] Recently it was found that in a subsequent oxidation step arsenolite can be further transformed into soluble arsenates. In their turn, these soluble species can migrate throughout the whole paint system, e.g., into the varnish layer, towards the interface between the paint layers and the ground, until they precipitate with suitable divalent or trivalent cations, such as calcium, lead, copper, aluminum, magnesium and iron.[33,36-39]

For this reason, both mimetite and schultenite encountered on the still life paintings are believed to be two of the possible end products of this multi-step alteration process for orpiment and/or realgar. Indeed, a paint sample taken from the lemon of *Festoon of Fruit and Flowers*, which exhibits a brownish appearance with whitish haze, revealed that lead arsenate needles have formed in the top surface of the paint as well as in the ground layer using SEM, ATR-FTIR and As-K edge XANES imaging.[37] It is noteworthy that in the still life paintings discussed here, the distribution of these two arsenates is quite different: schultenite is mainly formed in the lighter (highlighted) areas of the marigold, the lemon and the apricots, while mimetite has a more uniform distribution throughout the As-containing areas that have a greyish appearance (see Figure 3 and Figure S-6). This suggests that the formation of both arsenate minerals takes place in distinct conditions and/or is starting from different parent minerals.

Indeed, depending on the local chemical environment inside the paint layers either mimetite or schultenite formation will be favored. While schultenite is stable only in very acidic environments and with relatively high Pb^{II} and As^{V} concentrations ($K_{sp,25°C} \approx 10^{-23} - 10^{-24}$), the highly insoluble mimetite ($K_{sp,25°C} \approx 10^{-76} - 10^{-83}$) can already be formed in slightly acidic conditions with very dilute levels of Pb^{II} and As^{V}.[40,41] The lead white used in the ground and/or paint layers, or lead that was added as a siccative (e.g., lead oxide) can function as local sources of free Pb^{II}.[42]

Although previous paint sample analysis of the lemon showed intact orpiment particles together with arsenolite inside the yellow degraded paint layer,[37] neither orpiment nor realgar could be detected by means of MA-XRPD in any of the investigated areas. The low sensitivity of MA-XRPD for the arsenic sulfides, see Tables S2-3, might be insufficient to detect the diminished quantities of intact As_xY_x particles. Furthermore, the photo-oxidation products, pararealgar and

arsenolite, most commonly associated with orpiment and realgar degradation, are not found in our investigations. Since the sensitivity of XRPD to detect arsenic oxide is higher or in the same order as for the two lead arsenates, its absence indicates that (almost) all of the arsenic oxide has either undergone further oxidation or is present in the paint system in a dissolved (H_3AsO_3) or amorphous form.

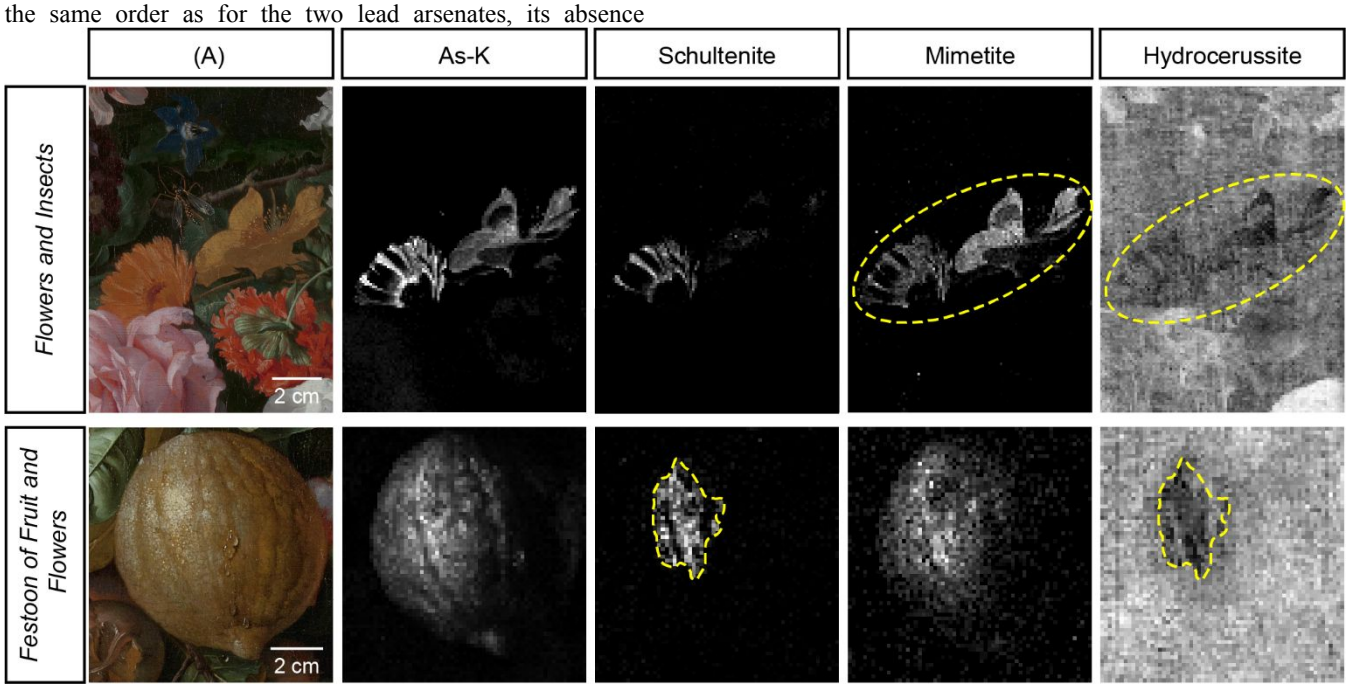

Figure 3. Details of (top) *Flowers and Insects* and (bottom) *Festoon of Fruit and Flowers* analyzed with MA-XRF/XRPD in transmission mode. (A) Optical photographs. Elemental distribution images of As-K and compound-specific distribution images of schultenite, mimetite and hydrocerussite. Brighter colors indicate a higher fluorescence intensity (MA-XRF) or scaling parameter (MA-XRPD). Experimental parameters are given in Table S-1.

The severity of this degradation process, mainly due to its ability to easily migrate throughout the entire paint system, is evidenced in the transmission data on *Flowers and Insects* and *Festoon of Fruit and Flowers*. Indeed, in areas that reveal a strong presence of schultenite or mimetite, the lead white distribution shows a clear loss in intensity (see yellow dashed lines in Figure 3 and Figure S-6). This is not an artefact because of an increase in attenuation of the primary or diffracted X-rays, but evidence of the depletion of lead white in the ground layer in favor of lead arsenate formation (see Figure S-8).

In the apricots of *Still Life with Fruit and a Lobster* and *Festoon of Fruit and Flowers*, the distribution of mimetite is either only or much more clearly visible in the reflection measurements (mimetite MA-XRPD maps in Figure S-6), indicating that (most of the) mimetite has manifested itself closely to the surface of these paintings. Since in this case the degradation has taken place only in the superficial paint layers, the lead white in the underlying ground does not seem to be affected.

Sulfates

In reflection mode, various (uncommon) secondary sulfates, palmierite ($K_2Pb(SO_4)_2$), syngenite ($K_2Ca(SO_4)_2.H_2O$) and gypsum ($CaSO_4.2H_2O$), are found at the surface of the copy painting *Still Life with Fruit and a Lobster*, while only palmierite is visible on (the surface of) *Flowers and Insects* and *Festoon of Fruit and Flowers* made by De Heem, see Figure 4 and Figure S-9.

Both syngenite and gypsum are frequently encountered weathering products in black crusts and efflorescence layers on stone monuments and mural paintings and as a white haze on medieval (K-rich) glass.[43-46] Potassium and sulfate originate either from internal (e.g., potash glass, K-rich feldspar in granite) or external sources (e.g., fertilizers, K-rich cement, KOH solutions for polychromy removal, dust particles and air pollution).[43,44,47,48] Depending on the available counter ions, sulfate salts with different composition will readily precipitate at the surface or inside cracks. The mention of syngenite in oil paintings seems very limited in literature: it has been found as a secondary salt in a red-orange Baroque bole ground used for the altar piece *Celebration of St. Roche*.[49] Only rarely, syngenite has been mentioned as a possible raw material in the plaster of a Chinese wall painting, together with calcite, quartz and gypsum.[50] Although gypsum can be an original material in oil paintings (e.g., as *gesso* ground in Southern European panel paintings, or mixed together with orpiment),[51] its presence at the surface of *Still Life with Fruit and a Lobster* seems to indicate its formation as a secondary product.

Palmierite, sometimes associated with anglesite ($PbSO_4$), has been found to a much lesser extent as a secondary sulfate on stone sculptures, medieval glass windows and wall paintings.[47,52,53] On the other hand, palmierite has been identified on several paintings from 17th century Old Masters such as Vermeer, Jordaens and Rembrandt.[54,55] The authors have also encountered palmierite in paint samples from works by Brueghel, Ensor and Rubens; in the latter it was found together with syngenite (unpublished data). The formation of palmierite has been proposed to follow a migration of Pb^{II}, originating from lead white, to the upper paint layers, where it can react with potassium from internal pigment sources (e.g., smalt, lake substrates and earth pigments) and sulfate from either environmental SO_2 or substrates such as alum.[54-57]

However, also lead driers could function as a source of free Pb^{II} ions.

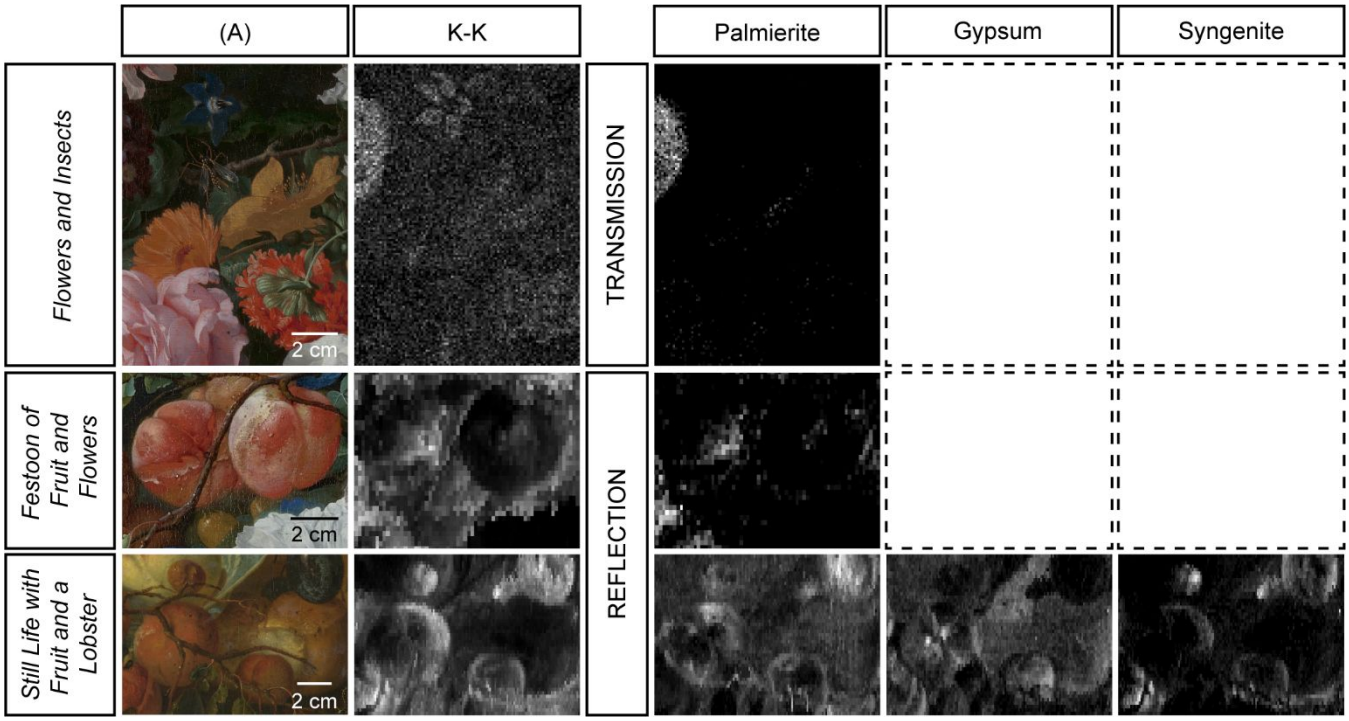

Figure 4. Elemental and compound-specific distribution images obtained with MA-XRF/XRPD in transmission or reflection mode from detailed areas of (top) *Flowers and Insects*, (middle) *Festoon of Fruit and Flowers*, and (bottom) *Still Life with Fruit and a Lobster*, showing K, Ca and several secondary formed (mixed) sulfates. Brighter colors indicate a higher fluorescence intensity (MA-XRF) or scaling parameter (MA-XRPD). Empty dashed boxes are shown when the respective compound was not detected. Experimental parameters are given in Table S-1. (A) Optical photographs of the analyzed areas.

In the results described here, the origin for the formation of these salts is twofold. On the one hand, palmierite formation has been confined to those regions where De Heem applied organic lakes. Indeed, in *Festoon of Fruit and Flowers* palmierite seems to have formed only in the orange-red lakes used for the apricots, while in *Flowers and Insects* this salt is present only in the purple primroses (palmierite MA-XRPD maps in Figure 4). Here, both potassium and sulfate ions likely originate from potash alum that is a frequently used substrate, especially for red lakes.[58] Surprisingly, while smalt, a K-rich glass already associated to palmierite formation,[54,57] is used in the foliage of *Festoon of Fruit and Flowers*, this secondary salt has not been formed in this region, indicating the absence of a sulfate source, both internal and external. On the other hand, in *Still Life with Fruit and a Lobster*, syngenite is linked to the darker/shadow regions of the apricots and to the blue plums for which organic lakes have been used, while palmierite and gypsum are found throughout significant parts of the analyzed area (see Figure 4 bottom row). In regions with a high palmierite signal, gypsum exhibits a low signal and *vice versa*, indicating a possible competition between the two double salts depending on the available internal ions (Pb^{II} or Ca^{II}). The widespread presence of these two salts suggests that not only local sources, but also atmospheric SO_2 has played a role in their formation. Next to the potash alum, other internal sources for potassium are present, such as smalt used in the foliage, or ultramarine used in the blue details (e.g. blue plum). This is evidenced by the extent at which potassium is present throughout the imaged areas (see K-K MA-XRF map in Figure 4).

CONCLUSIONS

It is clear that the choice for either transmission or reflection mode MA-XRPD strongly depends on the goal of the study. Transmission mode allows to probe the underlying layers enabling the visualization of underlying compositions and or compositional paint changes. However, the object in question should be transparent to the X-ray energy that is used, which excludes paintings with a thick or strongly absorbing substrate, such as works on wooden panels or copper plates. For the study of superficial (pictorial or degradation) layers, acquisitions in reflection mode are preferred in which contributions from the ground layers are suppressed. However, care should be taken, as the information depth achievable in reflection mode can be very limited (< 10 μm) depending on the paint layers. Additionally, degradation processes can also greatly affect underlying layers, as was shown to be the case for the degradation of orpiment and realgar: transmission mode MA-XRPD clearly illustrated the depletion of lead white present in the ground in favor of the formation of both schultenite and mimetite.

In this study we have shown that MA-XRPD in both transmission and reflection mode is able to reveal the presence of various alteration products on (the surface of) three 17th century flower still life paintings. Two different arsenate minerals, schultenite and mimetite, were encountered. They are shown to be the endproducts of the multistep alteration pathway of the arsenic sulfides, orpiment and realgar, and show the strong tendency of arsenate ions to precipitate with Pb^{II} ions. Other possible arsenates of Ca^{2+}, Cu^{2+} and Mg^{2+} that have been

reported in different art objects were not found.[33,38,39,59] This is consistent with recent findings of lead arsenate with MA-XRPD on other 17th century Dutch still life paintings by A. Mignon and M. Nellius (not yet published). It is noteworthy that the formation of schultenite in this study is limited to both original paintings.

In addition, a superficial layer consisting of several secondary sulfate salts (palmierite, syngenite and gypsum) covers the entire analyzed area of *Still Life with Fruit and a Lobster*, while only select areas rich in lakes showed the presence of the mixed potassium lead sulfate on *Flowers and Insects* and *Festoon of Fruit and Flowers*. Although this difference could indicate that the copy was made with materials of apparently lower quality, more likely the specific restoration and conservation history of the paintings and the exposures to different atmospheres will have played a crucial role.

The MA-XRF and MA-XRPD results presented here did not allow for a complete characterization of the lakes used throughout these artworks. In order to understand the role of the various lakes (e.g., madder, cochineal) and colorants (indigo) in the formation of these secondary sulfate salts, complementary analyses with VNIR reflectance imaging spectroscopy could be performed.

Nevertheless, the chemical images shown in this study indicate the significant value that MA-XRPD can bring to the field of cultural heritage, not only for the identification of artist's materials, but also for the detection of degradation products and secondary compounds formed within precious works of art. The technique could therefore be a valuable new tool to follow restoration and cleaning treatments *in situ* and to guide sampling campaigns to strategic areas based on the macroscopic distributions of the alteration products. Especially for investigating discoloration phenomena on very delicate works of art on which sampling is often prohibited, such as illuminated manuscripts, MA-XRPD could play an important role. MA-XRPD therefore expands the suit of complementary analytical (imaging) techniques that are at the disposal of conservation scientists, conservators and art historians. To increase the applicability of MA-XRPD towards larger, immoveable works of art, efforts are being made to construct a scanning system in reflection mode in which the instrument and not the object is translated during the imaging experiment.

ASSOCIATED CONTENT

Supporting Information

Additional information as noted in the text. The Supporting Information is available free of charge on the ACS Publications website.

Experimental setup, estimation and tables of relative sensitivity and information depth, scan parameters, cross-section photographs, additional distribution images, diffractograms and diffraction patterns (PDF)

AUTHOR INFORMATION

Corresponding Author

* Email: frederik.vanmeert@uantwerpen.be

Author Contributions

The manuscript was written through contributions of all authors. All authors have given approval to the final version of the manuscript.

Notes

The authors declare no competing financial interest.

ACKNOWLEDGMENT

The authors acknowledge financial support from BELSPO (Brussels) S2-ART and METOX projects, the NWO (The Hague) Science4Arts 'ReVisRembrandt' project and the GOA Project Solarpaint (University of Antwerp Research Council). The authors thank the Rijksmuseum, the Royal Museum of Fine Arts Antwerp, and their staff for the collaborations.

REFERENCES

(1) Coccato, A.; Moens, L.; Vandenabeele, P. *Heritage Sci.* **2017**, *5*.

(2) Schreiner, M.; Melcher, M.; Uhlir, K. *Anal. Bioanal. Chem.* **2007**, *387*, 737-747.

(3) Bersani, D.; Lottici, P. P. *J. Raman Spectrosc.* **2016**, *47*, 499-530.

(4) Prati, S.; Joseph, E.; Sciutto, G.; Mazzeo, R. *Acc. Chem. Res.* **2010**, *43*, 792-801.

(5) Janssens, K.; Alfeld, M.; Van der Snickt, G.; De Nolf, W.; Vanmeert, F.; Radepont, M.; Monico, L.; Dik, J.; Cotte, M.; Falkenberg, G.; Miliani, C.; Brunetti, B. G. In *Annual Review of Analytical Chemistry, Vol 6*, Cooks, R. G.; Pemberton, J. E., Eds.; Annual Reviews: Palo Alto, 2013, pp 399-425.

(6) Bertrand, L.; Cotte, M.; Stampanoni, M.; Thoury, M.; Marone, F.; Schoder, S. *Phys. Rep.* **2012**, *519*, 51-96.

(7) Trentelman, K. In *Annual Review of Analytical Chemistry, Vol 10*, Cooks, R. G.; Pemberton, J. E., Eds.; Annual Reviews: Palo Alto, 2017, pp 247-270.

(8) Alfeld, M.; Janssens, K.; Dik, J.; de Nolf, W.; van der Snickt, G. *J. Anal. At. Spectrom.* **2011**, *26*, 899-909.

(9) Ricciardi, P.; Delaney, J. K.; Facini, M.; Zeibel, J. G.; Picollo, M.; Lomax, S.; Loew, M. *Angew. Chem.-Int. Edit.* **2012**, *51*, 5607-5610.

(10) Alfeld, M.; de Viguerie, L. *Spectrochim. Acta, Part B* **2017**, *136*, 81-105.

(11) Alfeld, M.; Broekaert, J. A. C. *Spectrochim. Acta, Part B* **2013**, *88*, 211-230.

(12) Cucci, C.; Delaney, J. K.; Picollo, M. *Acc. Chem. Res.* **2016**, *49*, 2070-2079.

(13) Legrand, S.; Alfeld, M.; Vanmeert, F.; De Nolf, W.; Janssens, K. *Analyst* **2014**, *139*, 2489-2498.

(14) Casadio, F.; Daher, C.; Bellot-Gurlet, L. *Top. Curr. Chem.* **2016**, *374*.

(15) Lauwers, D.; Brondeel, P.; Moens, L.; Vandenabeele, P. *Philos. Trans. R. Soc. A-Math. Phys. Eng. Sci.* **2016**, *374*, 10.

(16) Dooryhée, E.; Anne, M.; Bardiès, I.; Hodeau, J. L.; Martinetto, P.; Rondot, S.; Salomon, J.; Vaughan, G. B. M.; Walter, P. *Appl. Phys. A* **2005**, *81*, 663-667.

(17) De Nolf, W.; Dik, J.; Van der Snickt, G.; Wallert, A.; Janssens, K. *J. Anal. At. Spectrom.* **2011**, *26*, 910.

(18) Vanmeert, F.; De Nolf, W.; De Meyer, S.; Dik, J.; Janssens, K. *Anal. Chem.* **2018**, *90*, 6436-6444.

(19) Vanmeert, F.; Hendriks, E.; Van der Snickt, G.; Monico, L.; Dik, J.; Janssens, K. *Angew. Chem.-Int. Edit.* **2018**, *57*, 7418-7422.

(20) Vanmeert, F.; De Nolf, W.; Dik, J.; Janssens, K. *Anal. Chem.* **2018**, *90*, 6445-6452.

(21) De Meyer, S.; Vanmeert, F.; Janssens, K.; Storme, P. In *6th Interdisciplinary ALMA conference*, Hradilova, J.; Hradil, D., Eds.; Academy of Fine Arts in Prague: Brno, 2017, pp 29-38.

(22) De Keyser, N.; Van der Snickt, G.; Van Loon, A.; Legrand, S.; Wallert, A.; Janssens, K. *Heritage Sci.* **2017**, *5*, 13.

(23) De Nolf, W.; Vanmeert, F.; Janssens, K. *J. Appl. Crystallogr.* **2014**, *47*, 1107-1117.

(24) Sole, V. A.; Papillon, E.; Cotte, M.; Walter, P.; Susini, J. *Spectrochim. Acta, Part B* **2007**, *62*, 63-68.

(25) Segal, S.; Helmus, L. *Jan Davidsz de Heem en zijn kring*; SDU: 's-Gravenhage, 1991.

(26) Hirayama, A.; Abe, Y.; van Loon, A.; De Keyser, N.; Noble,

P.; Vanmeert, F.; Janssens, K.; Tantrakarn, K.; Taniguchi, K.; Nakai, I. *Microchem. J.* **2018**, *138*, 266-272.
(27) Kakoulli, I. *Stud. Conserv.* **2002**, *47*, 56-67.
(28) Leona, M. *The Metropolitan Museum of Art Bulletin* **2009**, *67*, 7.
(29) Buisson, N.; Burlot, D.; Eristov, H.; Eveno, M.; Sarkis, N. *Archaeometry* **2015**, *57*, 1025-1044.
(30) Holakooei, P.; Karimy, A. H. *J. Archaeol. Sci.* **2015**, *54*, 217-227.
(31) Brecoulaki, H. *La peinture funéraire de Macédoine: emplois et fonctions de la couleur IVe-IIe s. av. J.-C.*: de Boccard, Paris, 2006.
(32) Hradil, D.; Hradilova, J.; Bezdicka, P.; Svarcova, S.; Cermakova, Z.; Kosarova, V.; Nemec, I. *J. Raman Spectrosc.* **2014**, *45*, 848-858.
(33) Keune, K.; Mass, J.; Meirer, F.; Pottasch, C.; van Loon, A.; Hull, A.; Church, J.; Pouyet, E.; Cotte, M.; Mehta, A. *J. Anal. At. Spectrom.* **2015**, *30*, 813-827.
(34) FitzHugh, E. W. In *Artists´ Pigments A Handbook of Their History and Characteristics*, FitzHugh, E. W., Ed.; Archetype Publications: London, 1997, pp 47-79.
(35) Douglass, D. L.; Shing, C. C.; Wang, G. *Am. Mineral.* **1992**, *77*, 1266-1274.
(36) Vermeulen, M.; Nuyts, G.; Sanyova, J.; Vila, A.; Buti, D.; Suuronen, J. P.; Janssens, K. *J. Anal. At. Spectrom.* **2016**, *31*, 1913-1921.
(37) Keune, K.; Mass, J.; Mehta, A.; Church, J.; Meirer, F. *Heritage Sci.* **2016**, *4*.
(38) Holakooei, P.; Karimy, A.-H.; Nafisi, G. *Stud. Conserv.* **2018**, 1-12.
(39) van Dyke, Y.; Centeno, S. A.; Caro, F.; Frantz, J. H.; Wypyski, M. T. *Heritage Sci.* **2018**, *6*, 9.
(40) Magalhaes, M. C. F.; Silva, M. C. M. *Monatsh. Chem.* **2003**, *134*, 735-743.
(41) Sjostedt, C.; Lov, A.; Olivecrona, Z.; Boye, K.; Kleja, D. B. *Appl. Geochem.* **2018**, *92*, 110-120.
(42) Cotte, M.; Checroun, E.; De Nolf, W.; Taniguchi, Y.; De Viguerie, L.; Burghammer, M.; Walter, P.; Rivard, C.; Salomé, M.; Janssens, K.; Susini, J. *Stud. Conserv.* **2017**, *62*, 2-23.
(43) Matović, V.; Erić, S.; Kremenović, A.; Colomban, P.; Srećković-Batoćanin, D.; Matović, N. *Journal of Cultural Heritage* **2012**, *13*, 175-186.
(44) Eric, S.; Matovic, V.; Kremenovic, A.; Colomban, P.; Batocanin, D. S.; Neskovic, M.; Jelikic, A. *Constr. Build. Mater.* **2015**, *98*, 25-34.
(45) Melcher, M.; Schreiner, M. *J. Non-Cryst. Solids* **2006**, *352*, 368-379.
(46) Vettori, S.; Bracci, S.; Cantisani, E.; Riminesi, C.; Sacchi, B.; D'Andria, F. *Microchem. J.* **2016**, *128*, 279-287.
(47) Prikryl, R.; Svobodova, J.; Zak, K.; Hradil, D. *Eur. J. Mineral.* **2004**, *16*, 609-617.
(48) Melcher, M.; Schreiner, M.; Kreislova, K. *Phys. Chem. Glasses: Eur. J. Glass Sci. Technol., Part B* **2008**, *49*, 346-356.
(49) Simova, V.; Bezdicka, P.; Hradilova, J.; Hradil, D.; Grygar, T. *Powder Diffr.* **2005**, *20*, 224-229.
(50) Zeng, Q. G.; Zhang, G. X.; Leung, C. W.; Zuo, J. *Microchem. J.* **2010**, *96*, 330-336.
(51) Eastaugh, N.; Valentine, W.; Chaplin, T.; Siddall, R. *Pigment Compendium - A dictionary and optical microscopy of historical pigments*; Butterworth-Heinemann, 2008, p 960.
(52) Sterpenich, J. *Bull. Eng. Geol. Environ.* **2002**, *61*, 179-193.
(53) Cotte, M.; Susini, J.; Solé, V. A.; Taniguchi, Y.; Chillida, J.; Checroun, E.; Walter, P. *J. Anal. At. Spectrom.* **2008**, *23*, 820.
(54) Van Loon, A.; Noble, P.; Boon, J. J. In *ICOM Committee for Conservation 16th Triennial Conference*: Lisbon, 2011.
(55) Price, S. W. T.; Van Loon, A.; Keune, K.; Parsons, A. D.; Murray, C.; Beale, A. M.; Mosselmans, J. F. W. *Chem. Commun.* **2019**, *55*, 1931-1934.
(56) Boon, J. J.; Oberthaler, E. In *Vermeer, Die Malkunst – Spurensicherung an einem Meisterwerk : Ausstellungskatalog des Kunsthistorischen Museums Wien*, Haag, S.; Oberthaler, E.; Pénot, S., Eds.; Residenz Verlag, 2010, pp 328-335.
(57) Boon, J. J. *Microsc. Microanal.* **2013**, *19*, 1408-1409.
(58) Kirby, J.; Spring, M.; Higgitt, C. *Natl. Gallery Tech. Bull.* **2005**, *26*, 71-87.
(59) Pages-Camagna, S.; Laval, E.; Vigears, D.; Duran, A. *Appl. Phys. A: Mater. Sci. Process.* **2010**, *100*, 671-681.

Authors are required to submit a graphic entry for the Table of Contents (TOC) that, in conjunction with the manuscript title, should give the reader a representative idea of one of the following: A key structure, reaction, equation, concept, or theorem, etc., that is discussed in the manuscript. Consult the journal's Instructions for Authors for TOC graphic specifications.